

Semiconductor defect metrology using laser-based quantitative phase imaging

Renjie Zhou^{a,b,c}, Chris Edwards^{a,b}, Gabriel Popescu^b, and Lynford L. Goddard^{*a}

^aMicro and Nanotechnology Laboratory, Department of Electrical and Computer Engineering
University of Illinois at Urbana-Champaign, Urbana, Illinois 61801, USA

^bQuantitative Light Imaging Laboratory, Department of Electrical and Computer Engineering
Beckman Institute for Advanced Science and Technology
University of Illinois at Urbana-Champaign, Urbana, Illinois 61801, USA

^cCurrently with George R. Harrison Spectroscopy Laboratory, Massachusetts Institute of
Technology, Cambridge, Massachusetts 02194, USA

*lgoddard@illinois.edu; phone 1 217 244-0799; fax 1 217 244-6375; <http://psl.mntl.illinois.edu>

ABSTRACT

A highly sensitive laser-based quantitative phase imaging tool, using an epi-illumination diffraction phase microscope, has been developed for silicon wafer defect inspection. The first system used a 532 nm solid-state laser and detected 20 nm by 100 nm by 110 nm defects in a 22 nm node patterned silicon wafer. The second system, using a 405 nm diode laser, is more sensitive and has enabled detection of 15 nm by 90 nm by 35 nm defects in a 9 nm node densely patterned silicon wafer. In addition to imaging, wafer scanning and image-post processing are also crucial for defect detection.

Keywords: Wafer defect inspection, interferometric microscopy, quantitative phase imaging, laser defect inspection, image post-processing

1. INTRODUCTION

Metrology is the science of measurement. Over the past years, the size of semiconductor device features has shrunk to the nanoscale. Thus, extremely high-precision measurement tools need to be developed. Due to the highly serialized nature of semiconductor manufacturing, metrology is playing an important role to ensure that wafers have not been damaged by previous processing steps. If defects are presented in a die, they may actually fail the whole circuit. Thus, it is essential to develop inline metrology tools to maximize the yield during the manufacturing. Inline detection of sub-10 nm killer defects in patterned wafers is a grand challenge, especially as the semiconductor industry moves beyond the 11 nm node, according to the 2013 International Technology Roadmap for Semiconductors report on metrology [1].

Compared with scanning electron microscopy (SEM) and atomic force microscopy (AFM), optical microscopy methods have high throughput and work in noncontact mode, thus, they are ideal for inline defect inspection and have been demonstrated earlier [2-4]. In a bright-field microscopy system, both the reflected and scattered photons are collected and measured as intensity distributions. Thus, it can be used for either patterned or unpatterned wafer inspection. Light source stability and system noise isolation are very crucial to achieve nanometer scale defect inspection sensitivity. In addition to light intensity measurements, interferometry, acting as a homodyne detection that amplifies a weak signal, has been added to bright-field to measure amplitude and phase of the scattered light from a small defect [4]. The phase information relates to the structure topography information. Over the past three years, we have developed a common-path laser interferometric microscopy system for quantitative phase imaging (QPI) and adapted it for defect inspection. Our system is based on an epi-illumination diffraction phase microscopy (epi-DPM) system, which was demonstrated to have < 1mrad phase sensitivity [5-7]. Using this system, we have successfully detected deep subwavelength defects in 32 nm node, 22 nm node, and 9 nm node patterned wafers [8-11].

The first version of the laser defect inspection system used a frequency-doubled Nd: YAG 532 nm solid-state laser and a 40x/0.9 objective (Zeiss EC Plan-Neofluar 40x/0.9 Pol). During the imaging, we scanned the wafer in plane and captured an image stack. Using the phase and amplitude images retrieved from the system and a comprehensive image post-processing method, we were able to detect different types of defects with sizes down to 20 nm by 100 nm by 110 nm in a 22 nm node patterned wafer. To address the inspection need in 9 nm node densely patterned wafers, we further improved the sensitivity and resolution by using a 405 nm diode laser with a Faraday rotator based isolator that had 10x better power stability than the 532 nm Nd: YAG laser. We also quantified the improvement in the spatial and temporal noise of the phase image. This update enabled detection of 15 nm by 90 nm by 35 nm defects in a 9 nm node densely patterned wafer.

Quantitative Phase Imaging, edited by Gabriel Popescu, YongKeun Park, Proc. of SPIE Vol. 9336,
933611 · © 2015 SPIE · CCC code: 1605-7422/15/\$18 · doi: 10.1117/12.2078329

2. 532 NM LASER INSPECTION

As illustrated in Fig. 1, the wafer defect image acquisition uses an epi-DPM system, which is based on a 532 nm laser common-path Mach-Zehnder interferometer. The system is immune to vibrational noise and can reconstruct amplitude and phase image in a single shot. Detailed experimental description can be found in reference [6, 10]. We have used this system for measuring a 22 nm node intentional defect array (IDA) wafer provided by SEMATECH. This wafer consists of 22 nm wide, 120 nm or 260 nm long, and 110 nm high line patterns. An SEM image of a portion of this IDA wafer is shown in the bottom left of Fig. 1. On this wafer, different types of defects (the bottom right images) are intentionally printed as indicated by the color boxes. The cross-section sizes of the defects are on the order of 20 nm by 100 nm. The epi-DPM system measures an interferogram, which is used to retrieve both the amplitude and phase of the scattered field from the sample using the Fourier transform method. To detect these small intentional defects, we need to further reduce the remaining noise in the images to amplify the defect signal to background contrast. In order to achieve that, we have developed image post-processing methods. We first collect a sequence of amplitude and phase images by translating the wafer in one direction parallel to the wafer surface with 0.75 micron steps. Then, we use the scanning images to produce 2nd order differential images to reduce spatial noise and also produce a tripole pattern for the defect. Next, we stitch the 2nd order differential images together to produce a stretched panoramic image to reduce temporal noise and system calibration errors. Finally, the stretched image is convolved with a matched tripole pattern to extract the defect and eliminate the background signal from the wafer's underlying structure. Previous results showed that we can reliably detect defects with sizes smaller than 20 nm by 100 nm by 110 nm in this wafer [9, 10].

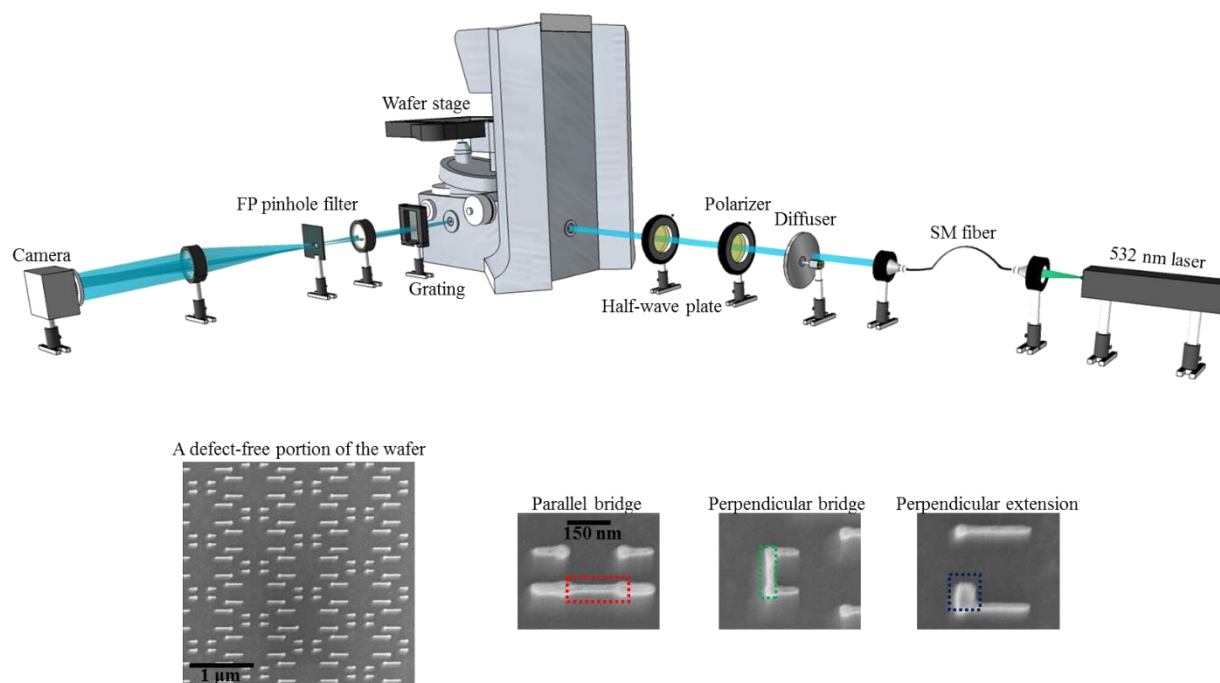


Figure 1. Illustration of the wafer defect inspection system. The top figure is the inspection system schematic. The bottom figures show the wafer pattern and different types of defects.

In the stitched 2nd order differential images, there is undesired underlying structure from the wafer pattern. In order to remove the underlying structure, a reference pattern is needed. Since the IDA wafer pattern is periodic, we can use it as a self-referenced pattern to cancel the underlying structure, leaving only the defect tripole pattern in the final stitched 2nd order differential images. Here, we show the steps of how to perform the self-referencing in the IDA wafer. We start with the scan amplitude images retrieved from the interferograms. Figures 2(a)-(c) show an example set of three adjacent frames with separation of 0.75 μm . The defect is marked by a red rectangular box. For self-referencing, we need to achieve 1.6 μm frame separations. This can be done simply by a digital shift of Fig. 2 (a) and (b) of 0.85 μm to the right and left, respectively. However, due to the translation stage stepping error, the actual shifting amount can be different.

Thus, we perform cross-correlation between Fig. 2(a) and (b), and Fig. 2(b) and (c) to find the exact shifting amount. With the cross-correlation method, we found that Fig. 2(a) needs 0.833 μm digital shifting to the right and Fig. 2(c) needs 0.786 μm digital shifting to the left. After the digital shifting, we produce a 2nd order differential image which is shown in Fig. 2(d) where the defect starts to become noticeable. We repeat this digital-shifting for all the scan frames, and produce a sequence of 2nd order differential images. Then, we stitch all the images together to produce a panoramic image as shown in Fig. 2(e). Now, we see that the defect to underlying structure signal ratio is very high, leading to clear detection of the defect in the 70 μm by 27 μm field of view. A tripole matched convolution can be performed on Fig. 2(e) to further enhance the defect signal. The image shows detection of a parallel bridge defect with 20 nm by 100 nm size which is also verified by SEM. We have also successfully applied this self-referencing method to the scan phase images.

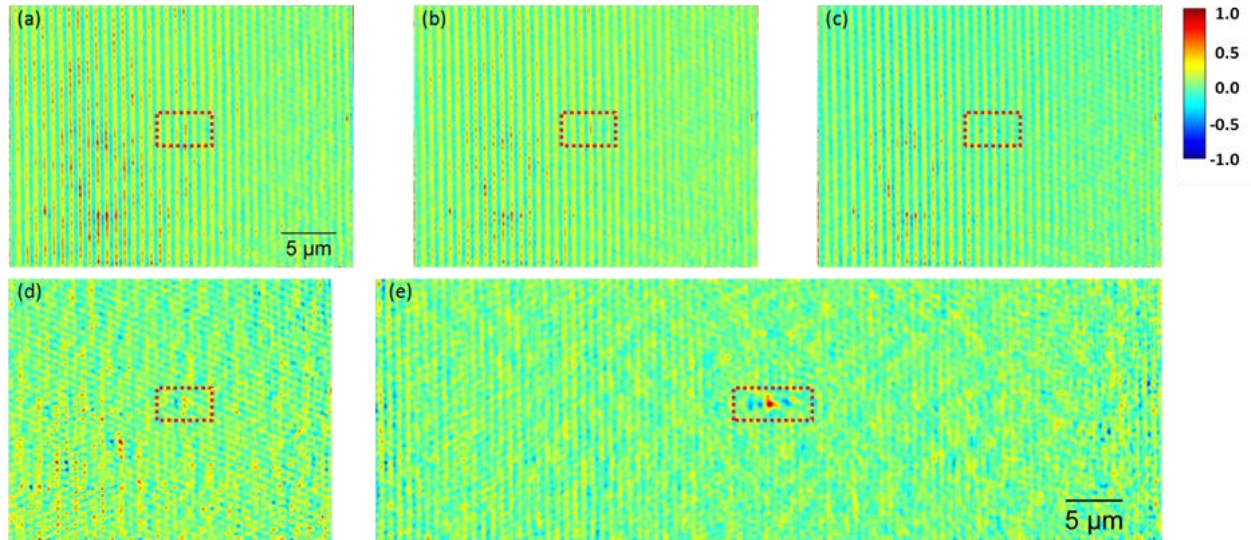


Figure 2. Illustration of pattern self-referencing. (a)-(c) is an example set of three adjacent amplitude images with 0.75 μm separation, (d) is the 2nd order differential after digital shifting with realization of 1.6 μm frame separation, and (e) is the panoramic 2nd order differential amplitude image after stitching. This detection image has a 20 nm by 100 nm parallel bridge defect which is verified by SEM.

3. 405 NM LASER INSPECTION

After inspection of the 22 nm node IDA wafer, we started inspecting a 9 nm node IDA wafer. This wafer has 9 nm by 270 nm periodic lines which are 2x denser than the previously examined 22 nm node IDA wafer, and the cross-section size of the defects are on order of 10 nm by 100 nm. Due to lack of the power stability of the 532 nm solid-state laser, we were unable to detect the intentional defects on this wafer. Thus, we decided to use a more stable 405 nm diode laser (QPhotonics QFLD-405-20S). This laser was measured to have a spectrum linewidth of about 2 nm at the imaging operation current of 60 mA. To further improve the laser power stability, we added a Faraday rotator based isolator after the laser to prevent back reflection of the light into the laser cavity. A 405 nm narrow-band filter was also installed on the camera window to remove the ambient light. To characterize the noise improvement, we measured the phase of a flat sample over time for 256 frames at two different field of views. We use the 256 frames at one field of view to compute the average phase calibration image for the 256 images at the other field of view, where we calculate the phase standard deviation at each pixel and obtained a histogram for the temporal noise and use all the pixel values of all the frames for the spatial noise histogram. In Fig. 3 we show the noise histogram with and without the isolator. Figure 3(a) and (c) are the spatial noise histogram without and with the isolator, respectively. Figure 3(b) and (d) are the temporal noise histogram without and with the isolator, respectively. From the histograms, we conclude that we have achieved spatial noise improvement from 6.92 nm to 1.65 nm and temporal noise improvement of 0.19 nm to 0.13 nm by using the isolator. When compared with the 532 nm laser with a diffuser, the 405 nm laser with isolator has an overall spatial noise that is reduced by 5.6x and a temporal noise that is reduced by 11.2x.

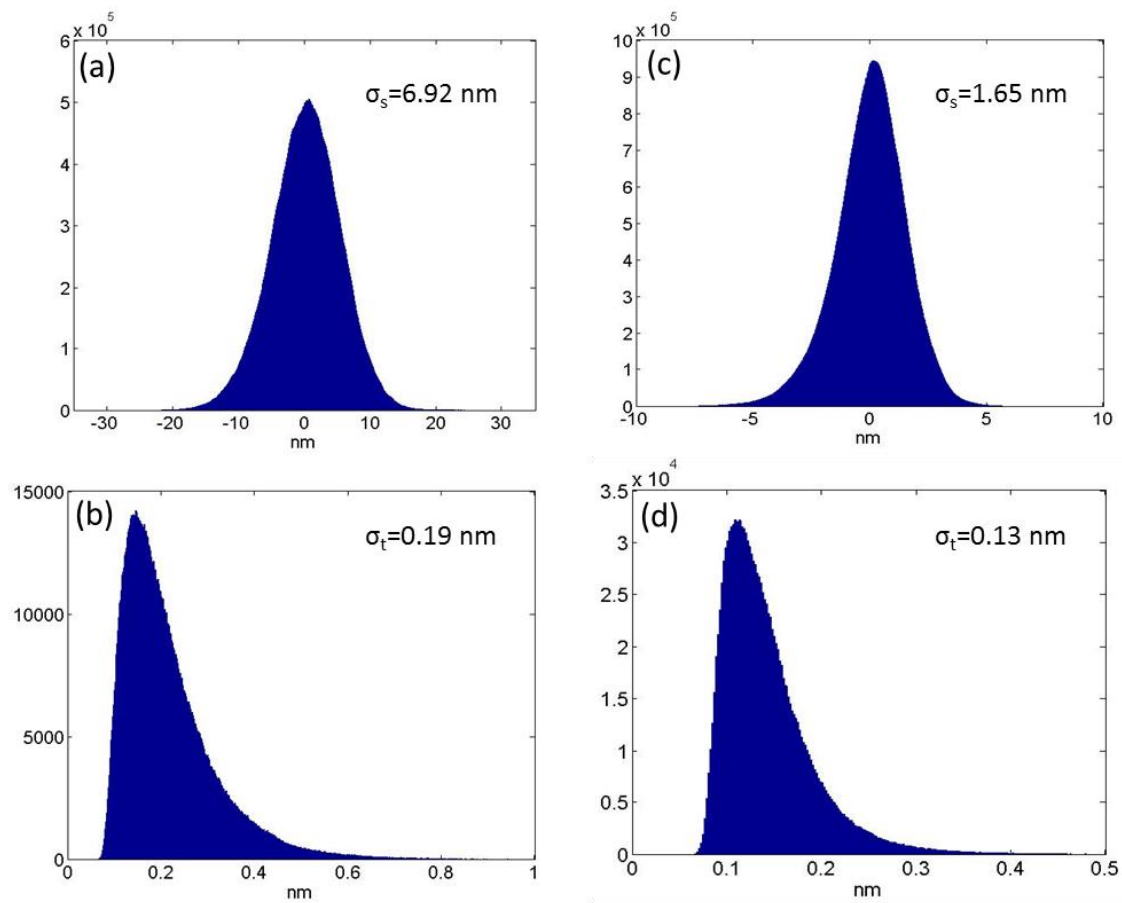


Figure 3. Noise characterization of the 405 nm diode laser. (a) The spatial noise histogram without the isolator. (b) The spatial noise with the isolator. (c) The temporal noise without the isolator. (d) The temporal noise with the isolator.

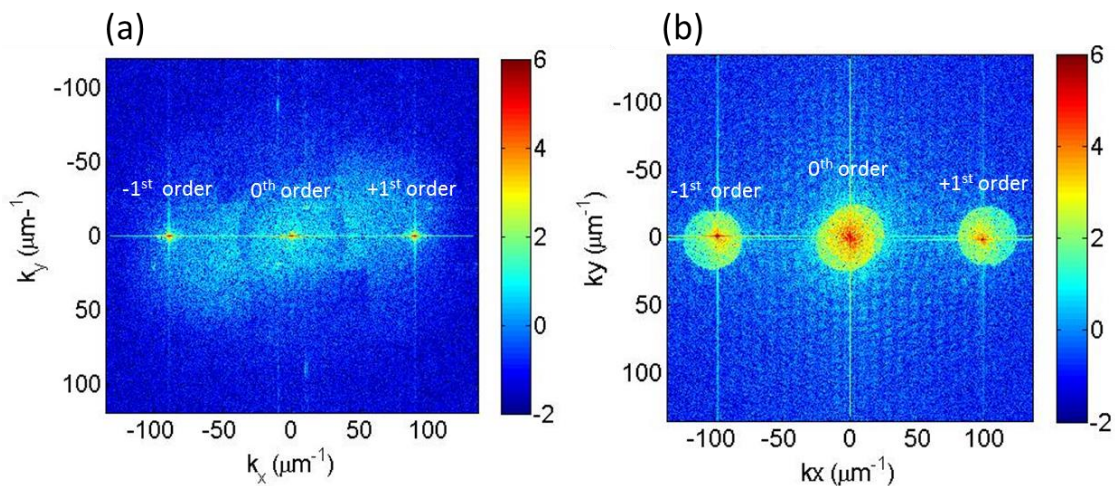


Figure 4. Comparison of the interferogram spectra from the 532 nm laser and the 405 nm laser. (a) 532 nm laser epi-DPM interferogram spatial spectrum. (b) 405 nm laser epi-DPM interferogram spatial spectrum.

The Fourier plane filter is another issue of the 532 nm laser DPM system, where we usually use a homemade cardboard cutout to roughly block the ambient light coming into the interference beam orders. To mitigate this problem, in the 405 nm laser system, we implemented a machined filter that exactly fits into the interference beam orders at this wavelength. With this filter, we were able to obtain interferograms with high fringe visibility. We compare the coupling of the ambient light for the 532 nm laser and the 405 nm laser in Fig. 4, where the magnitude of their interferogram Fourier spectra are plotted in log scale on a flat test sample. The Fourier components of the 532 nm laser, as shown in Fig. 4(a), are not distinct due to the ambient light coupling, while for the 405 nm laser the orders are very clear. Notice that in Fig. 4(b) the center of the +1st-order is not aligned with its maximum value which is due to the optical alignment error, which is estimated to be about 2%.

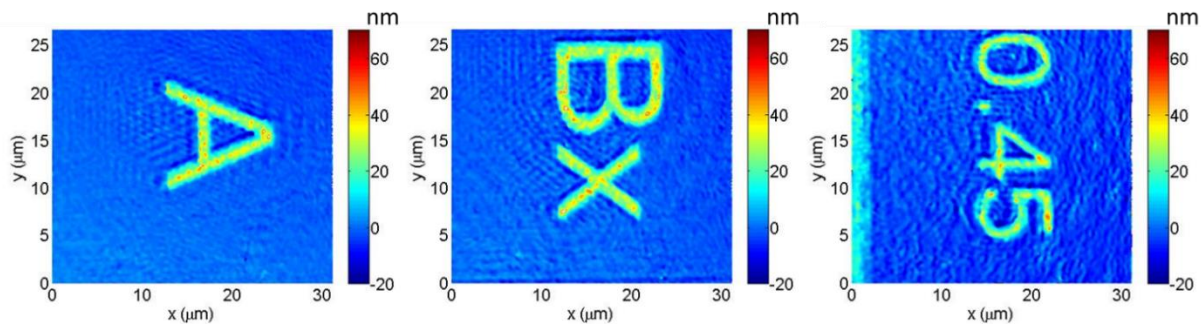


Figure 5. Surface profile measurements of letters and numbers on a 9 nm node silicon wafer.

After checking the interferogram spectra, we image the letter and number markers on a 9 nm node wafer, as we did for the 532 nm laser. The surface profiles for the letters are plotted in Fig. 5, where a feature height of about 50 nm is measured. After this test, we applied this system for the 9 nm IDA wafer defect measurement. We are able to measure defects with size smaller than 15 nm by 90 nm by 35 nm which are also verified with an Alpha-Step surface profiler and an oblique-angle SEM. The results will be presented in a following publication.

4. CONCLUSION

A wafer defect inspection tool based on laser epi-DPM has been demonstrated. This system is able to detect deep subwavelength defects on 22 nm node and 9 nm node patterned wafers. The success of defect detection is attributed to the common-path interferometry geometry, laser stability, and image post-processing. With a 10x more stable 405 nm diode laser, we are able to detect defects that are smaller than 15 nm by 90 nm by 35 nm in the 9 nm node wafer. In the future, we plan to engineer the Fourier filter planes at both the illumination and detection side to further enhance the system sensitivity.

ACKNOWLEDGMENTS

Semiconductor Research Corporation (contract P13117) and National Science Foundation (grant CBET-1040462 MRI) with matching funds from the University of Illinois are the major sponsors for this research. The Arnold and Mabel Beckman Foundation also supported the research through a graduate fellowship to RZ. We acknowledge SEMATECH for providing the test IDA wafers.

REFERENCES

- [1] <http://www.itrs.net/Links/2013ITRS/Summary2013.htm>.
- [2] Barnes, B. M., Sohn, Y.-J., Goasmat, F., Zhou, H., Silver, R. M. and Arceo, A., "Scatterfield microscopy of 22-nm node patterned defects using visible and DUV light," Proc. SPIE **8324**, 83240F (2012).
- [3] Barnes, B. M., Goasmat, F., Sohn, M. Y., Zhou, H., Silver, R. M. and Arceo, A., "Enhancing 9 nm node dense patterned defect optical inspection using polarization, angle, and focus," Proc. SPIE **8681**, 86810E (2013).
- [4] Schulze, M. A., Hunt, M. A., Voelkl, E., Hickson, J. D., Usry, W. R., Smith, R. G., Bryant, R. and Thomas, J. C. E., "Semiconductor wafer defect detection using digital holography," Proc. SPIE **5041**, 183-193 (2003).
- [5] Popescu, G., Ikeda, T., Dasari, R. R. and Feld, M. S., "Diffraction phase microscopy for quantifying cell structure and dynamics," Opt Lett **31**, 775-777 (2006).
- [6] Edwards, C., Arbabi, A., Popescu, G. and Goddard, L. L., "Optically monitoring and controlling nanoscale topography during semiconductor etching," Light Sci Appl **1**, e30 (2012).
- [7] Bhaduri, B., Edwards, C., Pham, H., Zhou, R., Nguyen, T. H., Goddard, L. L. and Popescu, G., "Diffraction phase microscopy: principles and applications in materials and life sciences," Adv Opt Photonics **6**, 57-119 (2014).
- [8] Zhou, R., Edwards, C., Popescu, G. and Goddard, L. L., "Diffraction phase microscopy for wafer inspection," in *Photonics Conference (IPC), 2012 IEEE*(2012), pp. 644-645.
- [9] Zhou, R., Popescu, G. and Goddard, L. L., "22 nm node wafer inspection using diffraction phase microscopy and image post-processing," SPIE **8681**, 86810G (2013).
- [10] Zhou, R., Edwards, C., Arbabi, A., Popescu, G. and Goddard, L. L., "Detecting 20 nm wide defects in large area nanopatterns using optical interferometric microscopy," Nano Lett **13**, 3716-3721 (2013).
- [11] Zhou, R., Edwards, C., Popescu, G. and Goddard, L. L., "9nm node wafer defect inspection using visible light," Proc. SPIE **9050**, 905017 (2014).